Extremely large thermal magnetoresistance and magnetic-field-driven transport-regime transition in macroscopic magneto-optical many-body systems

Lei Qu,[1,2] Svend-Age Biehs[1],[3] and Hong-Liang Yi[1],[1,2,*]

[1]*School of Energy Science and Engineering, Harbin Institute of Technology, Harbin 150001, People's Republic of China*

[2]*Key Laboratory of Aerospace Thermophysics, Ministry of Industry and Information Technology, Harbin 150001, People's Republic of China*

[3]*Institut für Physik, Carl von Ossietzky Universität, D-26111 Oldenburg, Germany*

Controlling near-field heat transport is crucial for the development of alternative energy applications. In recent years, the application of an external magnetic field to actively control noncontact heat transport has emerged as a highly appealing technique, and some exotic subwavelength-scale thermomagnetic phenomena have been predicted, especially in magneto-optical (MO) dipole systems. Here, we report two additional near-field thermomagnetic effects that can occur in macroscopic planar MO many-body systems. First, we predict an extremely large thermal magnetoresistance for nanoscale heat transport in a simple MO configuration comprising several interacting InSb planar slabs. It is found that the thermal resistance at room temperature can be substantially increased up to the order of 10 000% with a relatively strong magnetic field. We elucidate that this striking variation benefits from the multibody planar architecture, which allows us to transform an effective energy tunneling arising from zero-field cavity surface modes into a feeble tunneling mediated by field-induced hyperbolic modes. We also show the possibility of reducing the required field through structural optimization. Subsequently, we predict a magnetic-field-driven transition between superdiffusive and ballistic transport by further examining the radiative transport regime in a periodic InSb many-slab configuration under the action of external fields. This peculiar transition is associated with a field-induced alteration in the polarization of the dominant modes of transport. Our predicted thermomagnetic effects not only enrich the community of many-body energy transport but also provide guidelines for the development of advanced thermal management of elegant MO multibody architectures.

I. INTRODUCTION

Exploiting near-field electromagnetic energy is pivotal for various thermal applications, including thermophotovoltaics [1–3], photonic refrigeration [4,5], thermal diodes [6,7], etc. Motivated by these devices, significant progress has been made over the past decade in investigating and understanding radiative heat transport (RHT) between two bodies separated in the near-field regime [8–17]. In recent years, there has been emerging interest in exploring RHT in systems involving a set of interacting bodies [18–24]. These studies have already revealed the existance of plenty of peculiar transport phenomena that lack analogues in standard two-body systems, inspiring the creative design of advanced thermal functional devices with intrinsic many-body characteristics, such as near-field thermal transistors [25] and thermal routers [26,27].

One of the primary challenges confronting energy devices adopting either two- or many-body radiative configurations is to actively control and regulate their substantial photon-based fluxes in the near field. In this respect, some innovative ideas have been proposed in recent years and the interested reader can refer to recent reviews by Refs. [28–30]. One currently popular and appealing scenario is the use of an external magetic field in conjunction with mageto-optical (MO) materials [30,31]. Particular attention has been dedicated to magnetic semiconductors, including InSb, InAs, etc., since their strong MO activities are just located in the infrared band—a primary range for thermal radiation. Notably, some very intriguing near-field thermomagnetic effects have already been predicted, mainly based on many-body networks consisting of very small MO semiconductor spheres (usually regarded as dipoles). For example, when such spheres are meticulously arranged in a compact square configuration, the presence of an external static magnetic field can lead to the photon

---

*Corresponding author: yihongliang@hit.edu.cn

thermal Hall effect [31–33] as well as the persistent heat current in thermal equilibrium [19]. Besides, the thermal magnetoresistance (TMR) effect, a thermal analogue of the magnetoresistance (MR) effect in spintronics, has been revealed in a linear dipolar chain made of InSb [34]. By exposing this plasmonic network to a static magnetic field of several tesla, one demonstrated the existence of a TMR up to about 100%, which is analogous to the magnitude of the electronic giant MR (GMR) and therefore referred to as the giant TMR (GTMR) [34].

The MR (the dependence of electronic resistance on magnetic fields) is a key property, playing a crucial role in the development of spintronics and its applications [35–37]. Significant efforts in the field of spintronics are currently delicated to theoretically and experimentally uncover the existence of the extremely large MR (XMR, over 10^4%) in certain magnetic or nonmagetic materials [38–41], as well as in their associated layered structures [42,43], opening the way to the design of state-of-the-art magnetic devices. Such fascinating magnetoresistance phenomena, however, have not yet found their thermal counterparts thus far. Despite this, studies on the magnetic field dependence of thermal resistances have already made substantial progress during the past few years. Specifically, given that most energy-functional devices typically feature planar geometries, researchers have made numerous attempts to analyze and enhance the TMR in various macroscopic planar MO structures, but with a focus on two-body configurations. In a simplest situation where heat is radiatively transported between two identical infinite slabs made of *n*-doped InSb, Moncada-Villa *et al.* [11] showed that the presence of an externally static magnetic field always reduces the evanescent photon-based energy fluxes, allowing for the generation of a GTMR reaching about 230%. This magnetic field behavior on near-field RHT stems from the replacement of the surface polariton modes (evanescent within slabs as well as in vacuum), which dominate the zero-field RHT, by the field-induced hyperbolic modes (propagating within slabs but evanescent in vacuum), which are less efficient in transporting heat. They subsequently reported that this resistance magnitude is not very sensitive to the orientation of applied magnetic fields [44]. More recently, inspired by excellent photoelectric properties of MO topological media, researchers have found that near-field RHT between two magnetophotonic crystals can be more strongly inhibited in the presence of relatively strong magnetic fields, producing a huger thermal resistance [45–47]. For instance, when such structures are fabricated by alternating stacking of an InSb layer and a dielectric SiO_2 layer with appropriate thicknesses, the TMR value can be remarkably raised to around 500% by applying a background field up to 8 T. On the other hand, the magnetic field dependence of RHT has also been reported in several representative asymmetric MO systems, as a InSb slab separated by a
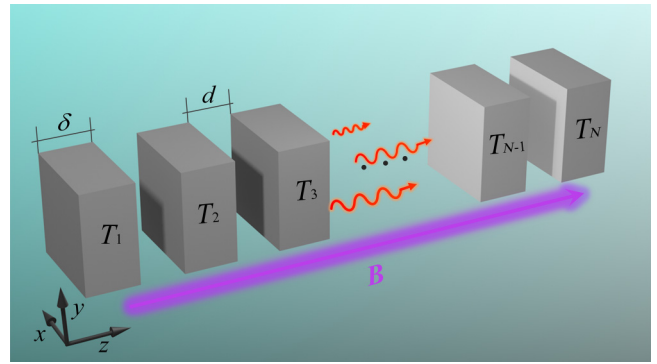

FIG. 1. Schematic drawing of a linear macroscopic system comprising of N parallel MO planar slabs with an identical thickness δ separated by vacuum gaps of size d, subjected to an external static magnetic field. These slabs are labeled with indices $1, \ldots, N$. Slab 1 and slab N are fixed at the temperatures $T_1 = T_N + \Delta T$ and $T_N = 300$ K using the two thermostats, while all the other slabs are left free to relax into their own temperature T_j.

vacuum gap from a Au slab [44] or graphene [48]. There, it has been demonstrated that the application of an external magnetic field is even capable of enhancing heat transport at the nanoscale (i.e., the so-called negative TMR effect), yet fails to induce a large (positive) thermal resistance, associated with the mismatch of resonance modes of dissimilar materials. Despite these remarkable steps forward, the reported TMR magnitude in existing planar MO configurations has never exceeded 1000%. Here, inspired by current advancements of MR in spintronics, we predict the existence of a thermal analogue of the XMR in the context of near-field RHT in a linear many-body architecture consisting of a few parallel planar slabs made of magnetic semiconductors (Fig. 1).

Another issue we are going to address in this study regarding this macroscopic MO system is its heat-transport regime. Unlike heat conduction in bulk solids, governed by a normal diffusion process, heat transport in systems where objects exchange energy via photons may exhibit anomalous (superdiffussive) behavior, offering an opportunity to design a new generation of composite materials or structures with the capacity to transport heat faster. In a pioneering study in 2013, Ben-Abdallah *et al.* [49] demonstrated the existence of a superdiffussive regime of transport in plasmonic networks of many interacting small spheres (working within the dipolar approximation), and displayed this anomalous transport process is independent of the system density. Notably, the Boltzmann transport equation cannot be safely applied in such systems [50]. During the years that followed, several studies further reported that the occurance of superdiffussive transport in many-dipole systems is not subjetcted to material components [51,52]. However, to date, studies on radiative transport regimes in macroscopic many-body systems

remain very scarce [53]. In Ref. [53], it has been shown that in a linear many-slab configuration purely made of dielectric SiC, a transition from superdiffusive to ballistic transport takes place as the entire system gets very dense, traced to a fundamental change of dominant modes (from TM- to TE-polarized modes). This finding suggests that the tranport rate of heat can be further elevated making use of a periodic planar multibody architecture, which is of significance for developing ultrafast thermal management. Neverthelsss, achieving such a transition through precise adjustments of structural parameters of complex architectures undoubtly poses immense challenges in both experimental verification and practical applications. From this perspective, an active control scenario could be urgently required. On the other hand, given the fact that SiC supports quite strong surface phonon polaritons [54,55], one might doubt whether ballistic transport persists in dense radiative many-slab systems made of certain media with similar properties. Taking into consideration two aforementioned aspects, our thoughts instinctively gravitate towards magnetic semiconductors, since, as mentioned before, they typically support strong surface modes in the absence of magnetic fields and, what is more, their surface states can be significantly affected upon applying an experimentally available magnetic field. These features motivate us to examine how heat carried by thermal photons is transported in a planar multibody configuration made of such MO media, as well as whether the application of a magnetic field allows one to induce a transition of transport regimes.

In this work, we predict two novel near-field thermomagnetic effects that can take place in macroscopic planar multibody systems made of MO semiconductors. Firstly, we find that the resistance of heat transported in a simple configuration, comprising just a few subwavelength-separation InSb planar slabs, can be as high as around 10 000% in the presence of a magnetic field up to 8 T, in the spirit of the XMR in spintronics. This phenomenon, which we term the extremely large thermal magnetoresistance (XTMR), profits by the many-body planar architecture, which permits an energy tunneling governed by zero-field cavity surface modes to be converted into a much less efficient tunneling mediated by magnetic-field-induced hyperbolic modes. We also demonstrate that it is possible to lower the required field by adjusting structural parameters such as the number of MO slabs.

Subsequently, we examine radiative transport regimes in the more complex InSb many-slab configuration, with a specific focus on the possibility of modifying transport regimes upon applying magnetic fields. It is shown that increasing the density of the considered MO system at zero fields leads to a transition in heat transport from a superdiffusive regime to a diffusion-like regime, in stark contrast to what was reported in the SiC many-slab case [53], showing that the heat-transport regime in planar multibody

systems depends not only on structural parameters but also on material components. More importantly, we demonstrate that the application of an external magnetic field is capable of inducing a transition between superdiffusive and ballistic transport. This field-driven transition (another field-induced phenomenon we predict) is found to be associated with a change in the dominant modes from TM- to TE-polarized modes, governing superdiffusive and ballistic regimes, respectively. We point out that although this finding agrees with that previously observed in the dielectric SiC architecture [53], the physical mechanism behind the magnetic-field-induced transition is more complex. It is worth noting that the thermomagnetic phenomena predicted here for the case of InSb are also expected to occur for other polar semiconductors like GaAs, InAs, etc., or even nonpolar semiconductors like Si. Our findings could have significant implications for the nanoscale thermal management of multibody architectures using external fields.

The remainder of this paper is organized as follows. Section II presents a description of the physical system under study. In Sec. III, we introduce the recently developed Green's function approach that we use to calculate radiative heat transport in planar MO many-body systems in the presence of an external magnetic field. Section IV is devoted to uncovering the XTMR effect in simple MO architectures comprising several noncontact InSb planar slabs. In Sec. V, we turn our attention to heat-transport regimes in the InSb many-slab configuration, particularly showing the possibility of a magnetic-field-induced transition between superdiffusive and ballistic regimes. In Sec. VI, we give some remarks on potential applications of our predicted thermomagnetic effects. Finally, the main conclusions of our work are summarized in Sec. VII.

II. PHYSICAL SYSTEM

Our current major task is to characterize heat transport in the system under consideration, consisting of N parallel MO semiconductor planar slabs separated by equal vacuum gaps of size d, subjected to an external static magnetic field **B**, as depicted in Fig. 1. These slabs, labeled with indices $1, \ldots, N$, have an identical thickness δ and, are assumed to be orthogonal to the z axis and infinite in both x and y directions so that the localized electromagnetic modes at their edges and corners play a negligible role in heat transport [56,57]. The temperatures of the two terminals, i.e., the hot slab 1 and cold slab N are fixed at $T_1 = T_N + \Delta T$ and $T_N = 300$ K, respectively, while all the other slabs are allowed to reach their own equilibrium temperature T_j $(j = 2, \ldots, N-1)$. In this study, we choose n-doped InSb as an example of magnetic semiconductors, and consider an external magnetic field, which is applied perpendicularly to the surface of the InSb slabs,

i.e., $\mathbf{B} = B\hat{z}$. We note that the alteration of the field orientation does not radically change the radiation property of planar InSb [44]. When exposed to an external field oriented as $\mathbf{B} = B\hat{z}$, InSb exhibits an optical anisotropy described by the following dielectric permittivity tensor [58]:

$$\hat{\varepsilon}_{\text{InSb}} = \begin{bmatrix} \varepsilon_1 & -i\varepsilon_2 & 0 \\ i\varepsilon_2 & \varepsilon_1 & 0 \\ 0 & 0 & \varepsilon_3 \end{bmatrix}, \quad (1)$$

where

$$\varepsilon_1(B) = \varepsilon_\infty \left(1 + \frac{\omega_L^2 - \omega_T^2}{\omega_T^2 - \omega^2 - i\Gamma\omega} + \frac{\omega_p^2(\omega + i\gamma)}{\omega[\omega_c^2 - (\omega + i\gamma)^2]} \right),$$

$$\varepsilon_2(B) = \frac{\varepsilon_\infty \omega_p^2 \omega_c}{\omega[(\omega + i\gamma)^2 - \omega_c^2]}, \quad (2)$$

$$\varepsilon_3 = \varepsilon_\infty \left(1 + \frac{\omega_L^2 - \omega_T^2}{\omega_T^2 - \omega^2 - i\Gamma\omega} - \frac{\omega_p^2}{\omega(\omega + i\gamma)} \right).$$

Here, $\varepsilon_\infty = 15.7$ is the high-frequency permittivity, $\omega_L = 3.62 \times 10^{13}$ rad s^{-1} ($\omega_T = 3.39 \times 10^{13}$ rad s^{-1}) is the longitudinal (transversal) phonon frequency, $\omega_p = 3.14 \times 10^{13}$ rad s^{-1} is the plasma frequency, and $\Gamma = 5.65 \times 10^{11}$ rad s^{-1} ($\gamma = 3.39 \times 10^{12}$ rad s^{-1}) is the phonon (free carrier) damping constants. The effect of the magnetic field is characterized by the cyclotron frequency $\omega_c = eB/m^*$, where $m^* = 1.99 \times 10^{-32}$ kg is the effective mass corresponding to a doping level of 1.07×10^{17} cm^{-3}.

Without external magnetic fields ($B = 0$), $\varepsilon_1 = \varepsilon_3$ and $\varepsilon_2 = 0$, so InSb is optically isotropic. In this case, the interface between the InSb slab and vacuum can support both surface plasmon polaritons (SPPs) at the frequencies below the surface plasmon frequency $\omega_{\text{SPP}} = \omega_p/\sqrt{2}$ and surface phonon polaritons (SPhPs) within the reststrahlen band $\omega_L < \omega < \omega_T$ [58]. These modes are characterized by an evanescent field in both InSb and vacuum, with a large component of wave vectors parallel to the interfaces, responsible for a strong transport of heat. When the magnetic field is turned on ($B \neq 0$), the MO effects are induced due to the generation of the complex off-diagonal elements, ε_2. And, in certain frequency regions another type of electromagnetic mode appears. These modes are referred to as hyperbolic modes (HMs) and classified as type I hyperbolic modes (HMI) with $\varepsilon_1 > 0$ and $\varepsilon_3 < 0$ and type II (HMII) with $\varepsilon_1 < 0$ and $\varepsilon_3 > 0$, as illustrated in Ref. [11]. These HMs are propagating within InSb but evanescent in vacuum, and their components of the wave vector parallel to the interfaces are much smaller than those of zero-field surface modes, rendering them less efficient to exchange heat between two infinite InSb slabs.

Let us now consider the radiative energy flux transported between two arbitrary MO slabs in the system under consideration. Given the stable nonreciprocity of InSb subjected to magnetic fields [19,32], the net flux

exchanged between slab i and slab j must be calculated by the following Landauer-like expression [29,34]:

$$\varphi_{ij} = \int_0^\infty \frac{d\omega}{2\pi} \int_{-\infty}^\infty \frac{d\mathbf{k}}{(2\pi)^2} [\Theta_i(\omega, T_i)\mathcal{T}_{i\to j}(\mathbf{k}, \omega)$$
$$- \Theta_j(\omega, T_j)\mathcal{T}_{j\to i}(\mathbf{k}, \omega)], \quad (3)$$

where $\Theta_i(\omega, T_i) = \hbar\omega/[\exp(\hbar\omega/k_B T_i) - 1]$ is the mean energy of photons with frequency ω, $\mathbf{k} = (k_x, k_y)$ is parallel wave vectors at temperature T_i, and $\mathcal{T}_{i\to j}(\mathcal{T}_{j\to i})$ denotes the transmission (tunneling) probability for the thermal photons from slab i to slab j (slab j to slab i), whose calculation will be given in the next section.

III. THEORETICAL APPROACH

Most prior studies on near-field heat transport in many-body systems with planar geometry have involved only isotropic or uniaxial materials (with the optical axis parallel to the transport direction) [23–25,53,59–63]. The photonic transmission probability in such systems is usually calculated using the analytical formula derived from the scattering approach [22,64,65]. This analytical formula, however, is not applicable to calculate the tunneling probability in the many-slab case involving anisotropic media (e.g., MO materials [19,32], Weyl semimetals [27], and so on) because the permittivity tensor of these materials has complex off-diagonal components. Here, we choose to utilize a Green's function approach [66,67] recently developed for the analysis of radiative energy transport in planar many-body systems made of materials with complex optical anisotropy.

Before implementing the Green's function approach, a key step is to establish the spatial positions of objects involved in the system. The assumption that the MO planar slabs are infinite along the x and y directions allows us to treat the system of Fig. 1 as a layered structure in the z direction, which, as sketched in Fig. 2, consists of alternating vacuum layers (green areas) and InSb layers (gray areas). By doing so, these layers can be labeled by l, extending from z_l to z_{l+1}.

As an example, let us now consider the situation where the flux is radiatively transported from the emitting layer e to the receiving layer r, as sketched in Fig. 2. In order to compute the photonic transmission probability between these two layers, we need to first determine the one at the two boundaries of layer r. For this, we are going to calculate the flux reaching arbitrary position z within layer r, generated from the fluctuating current sources within layer e (with a thickness δ), given by the z component of the Poynting vector

$$\varphi_{e\to z}(\mathbf{r}, t) = S(\mathbf{r}, z, t) = \hat{\mathbf{z}} \cdot \langle \mathbf{E}(\mathbf{r}, z, t) \times \mathbf{H}(\mathbf{r}, z, t) \rangle, \quad (4)$$

where $\langle \cdots \rangle$ denotes the ensemble average, $\mathbf{E}(\mathbf{r}, z, t)$ and $\mathbf{H}(\mathbf{r}, z, t)$ are the electric and magnetic fields, and $\mathbf{r} = (x, y)$
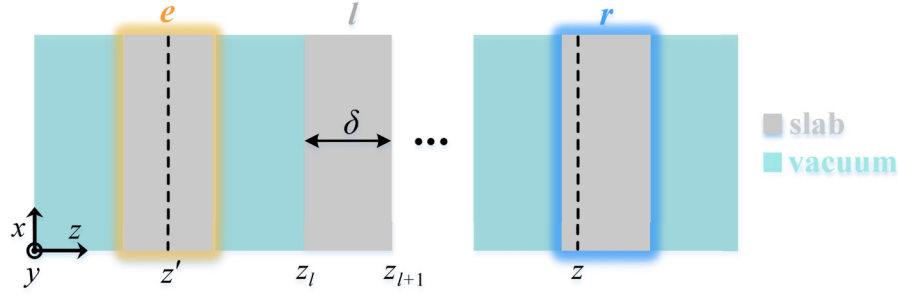
FIG. 2. Schematic drawing of a layered structure comprising alternating vacuum layers (green areas) and InSb layers (gray areas). Each layer can be labeled by l, extending from z_l to z_{l+1}. Thermal emission of fluctuating currents contained in the z' plane in layer e, is absorbed by the z plane in the receiving layer, r.

and t denote the in-plane coordinate and time, respectively. By using the time and space Fourier transforms, together with that $S(\mathbf{r}, z, t)$ is independent of $\mathbf{r}$ by translational symmetry, independent of z due to energy conservation and independent of t since the thermal process is a stationary random process [68], Eq. (4) can be rewritten as

$$S(z) = \frac{1}{2} \int_0^\infty d\omega \int_{-\infty}^{-\infty} \frac{d\mathbf{k}}{(2\pi)^4}$$
$$\times \mathrm{Re} \left\{ \hat{\mathbf{z}} \cdot \langle \mathbf{E}(\mathbf{k}, z, \omega) \mathbf{H}^*(\mathbf{k}, z, \omega) \rangle \right\}. \quad (5)$$

For the convenience of calculations, we recast Eq. (5) into the following form:

$$S(z) = \frac{1}{2} \int_0^\infty d\omega \int_{-\infty}^\infty \frac{d\mathbf{k}}{(2\pi)^4}$$
$$\times \mathrm{Re} \left\{ \mathrm{Tr} \left[\hat{\Gamma} \left\langle \mathbf{E}(\mathbf{k}, z, \omega) \mathbf{H}(\mathbf{k}, z, \omega)^* \right\rangle \right] \right\}. \quad (6)$$

Here, the matrix

$$\hat{\Gamma} = \begin{bmatrix} 0 & -1 & 0 \\ 1 & 0 & 0 \\ 0 & 0 & 0 \end{bmatrix},$$

and $\langle \mathbf{E}\mathbf{H}^* \rangle = \langle \mathbf{E}_\alpha \mathbf{H}_\beta^* \rangle$, where α and β represent the Cartesian components. The thermally generated electric and magnetic fields in the preceding equation can be calculated by the sum of the contributions stemming from the fluctuating current sources, $\mathbf{J}(\mathbf{k}, z', \omega)$, at all z' planes within layer e as

$$\mathbf{E}(\mathbf{k}, z, \omega) = \int_{z_e}^{z_e + \delta} dz' \hat{G}_E(\mathbf{k}, z, z', \omega) \mathbf{J}(\mathbf{k}, z', \omega), \quad (7)$$

$$\mathbf{H}(\mathbf{k}, z, \omega) = \int_{z_e}^{z_e + \delta} dz' \hat{G}_H(\mathbf{k}, z, z', \omega) \mathbf{J}(\mathbf{k}, z', \omega), \quad (8)$$

where $\hat{G}_E (\hat{G}_H)$ is the electric (magnetic) Green's function, which connects the emitting sources in a plane located at

position z' in the emitting layer e, with the absorbing plane at position z in the receiving layer r. The Green's functions can be solved by using the scattering matrix formalism [69]. More computational details can be found within the Supplemental Material [70].

From Eqs. (6)–(8) it is clear that the heat-flux calculation involves the ensemble average of the spatial correlation function of $\mathbf{J}$ within layer e, which can be given by the fluctuation-dissipation theorem [68]

$$\langle \mathbf{J}(\mathbf{k}, z, \omega) \mathbf{J}^\dagger(\mathbf{k}', z', \omega) \rangle$$
$$= (2\pi)^2 \frac{4}{\pi} \omega \varepsilon_0 \Theta(\omega, T_e) \frac{\hat{\varepsilon} - \hat{\varepsilon}^\dagger}{2i} \delta(\mathbf{k} - \mathbf{k}') \delta(z - z'), \quad (9)$$

where T_e and $\hat{\varepsilon}$ are the temperature and the permittivity tensor of the emitting layer e, respectively. Notably, although Eq. (9) is strictly derived from thermal-equilibrium systems, it is still possible to apply it to systems out of thermal equilibrium by assuming local thermal equilibrium [71].

Plugging Eqs. (7)–(9) into Eq. (6), we obtain the following expression for the radiative heat flux at position z within the receiving layer r:

$$S(z) = \int_0^\infty \frac{d\omega}{2\pi} \int_{-\infty}^\infty \frac{d\mathbf{k}}{(2\pi)^2} 4\omega\varepsilon_0 \Theta(\omega, T) \int_{z_e}^{z_e + \delta} dz'$$
$$\times \mathrm{Re} \left\{ \mathrm{Tr} \left[\hat{\Gamma} \hat{G}_E(\mathbf{k}, z, z', \omega) \frac{\hat{\varepsilon} - \hat{\varepsilon}^\dagger}{2i} \hat{G}_H^\dagger(\mathbf{k}, z, z', \omega) \right] \right\}. \quad (10)$$

Comparing this expression to Eq. (3), it is easy to identify the z-position photonic transmission probability

$$\mathcal{T}(\mathbf{k}, z, \omega) = 4\omega\varepsilon_0 \, \mathrm{Re} \int_{z_e}^{z_e + \delta} dz'$$
$$\times \left\{ \mathrm{Tr} \left[\hat{\Gamma} \hat{G}_E(\mathbf{k}, z, z', \omega) \frac{\hat{\varepsilon} - \hat{\varepsilon}^\dagger}{2i} \hat{G}_H^\dagger(\mathbf{k}, z, z', \omega) \right] \right\}. \quad (11)$$

Note that Eq. (11) allows for calculating the transmission probability from the emitting layer e to any positions z

within the receiving layer r, which is another advantage of the Green's function approach over the scattering approach (the latter can only capture the transmission probability between layers). Finally, the transmission probability between layer e and layer r, $\mathcal{T}_{e\rightarrow r}(\mathbf{k}, \omega)$, can be obtained by the difference in the one at the two boundaries of layer r.

Let us finish this section by saying that the numerical simulation for the MO system we consider has shown that $\mathcal{T}_{i\rightarrow j}(\mathbf{k}, \omega) = \mathcal{T}_{j\rightarrow i}(\mathbf{k}, \omega)$. Such a reciprocity of the transmission probability is consistent with the results reported in Ref. [34] for a linear chain of InSb nanospheres. We also note that the radiative transport reciprocity in nonreciprocal many-body systems can be analytically demonstrated by the symmetry of the magnetic group and the second law of thermodynamics, as shown in Ref. [72]. With this in mind, Eq. (3) can be simplified as follows:

$$\varphi_{ij} = \int_0^\infty \frac{d\omega}{2\pi} \int_{-\infty}^\infty \frac{d\mathbf{k}}{(2\pi)^2} [\Theta_i(\omega, T_i) \\ - \Theta_j(\omega, T_j)] \mathcal{T}_{i\rightarrow j}(\mathbf{k}, \omega). \quad (12)$$

To simplify the analytic treatment, we consider the situation where the temperature difference ΔT between the two terminals is small, namely, the temperature of slab 1 is only slightly higher than that of slab N. This thereby guarantees that the temperature differences involved in the entire system are sufficiently small, so that we can introduce the linear conductance or the heat-transfer coefficient h_{ij}, expressed as

$$h_{ij} = \lim_{T_i - T_j \rightarrow 0} \frac{\varphi_{ij}}{T_i - T_j} = \int_0^\infty \frac{d\omega}{2\pi} \int_{-\infty}^\infty \frac{d\mathbf{k}}{(2\pi)^2} \\ \times \frac{\partial \Theta(\omega, T_j)}{\partial T_j} \mathcal{T}_{i\rightarrow j}(\omega, \mathbf{k}). \quad (13)$$

Here, we note that T_j is the equilibrium temperature of slab j, which can be obtained by solving a set of the energy balance equation $\sum_{\substack{i \neq j \\ j \neq (1,N)}} \varphi_{ij} = 0$ using an iterative procedure based on the Jacobian matrix [52,61]. Hereafter, we employ Eq. (13) to analyze the thermal resistance (see Sec. IV) and the heat-transport regime (see Sec. V) in the MO architecture under study without and with an external magnetic field.

IV. EXTREMELY LARGE TMR IN MO FEW-SLAB CONFIGURATIONS

As mentioned in the Introduction, most previous studies on the analysis of the TMR in planar MO systems have been limited to two-body cases [11,44–58]. In this section, we shall unveil the extent to which thermal resistance can be affected by an external magnetic field in the MO many-body architecture of Fig. 1. According to the definition of
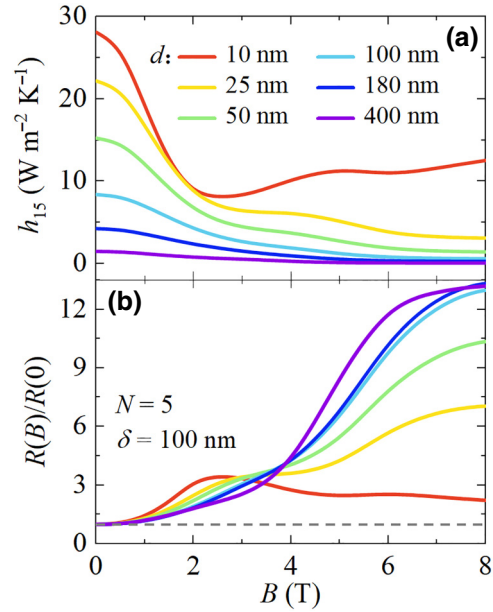

FIG. 3. (a) Heat-transfer coefficient h_{15} of a few-body architecture consisting of $N = 5$ InSb planar slabs with a thickness of 100 nm as a function of the magnetic field intensity B for various gap sizes d. (b) Ratio of the thermal resistance $R(B)/R(0)$ at finite fields to the one at zero fields versus the magnetic field intensity for the considered gap sizes. Gray dashed lines correspond to $R(B)/R(0) = 1$. The temperature of the cold terminal (i.e., slab 5) is fixed at 300 K.

thermal resistances in linear networks [34], the (largest) resistance of the considered MO architecture in the presence of magnetic fields is given by $R(B) \equiv R_{1N}(B) = h_{1N}^{-1}(B)$. Then, the TMR can be expressed following the electronic magnetoresistance concept as

$$\text{TMR} = \frac{R(B) - R(0)}{R(0)} \times 100\%, \quad (14)$$

where $R(0)$ is the thermal resistence without magnetic fields. Obviously, the presence of the intermediate slabs (with indices $2, \dots, N - 1$) will affect the travel of thermal photons between the hot slab 1 and the cold slab N, i.e., they are funicitioning as energy modulators.

Let us start the discussion by considering a simple geometry, which consists of $N = 5$ InSb planar slabs with the same thickness $\delta = 100$ nm. These two structural parameters are used in this section unless otherwise mentioned. Figure 3(a) shows the heat-transfer coefficient h_{15} versus the magnetic field intensity B for different values of the gap size d. In the absence of a magetic field ($B = 0$), we see an expected significant decrease in the transfer coefficient with increasing d, associated with the evanescent nature of surface modes that dominate near-field energy fluxes. Now, when an external magnetic field is applied, it is clearly observed that the transfer coefficient for a sufficiently small gap of 10 nm exhibits a nonmonotonic
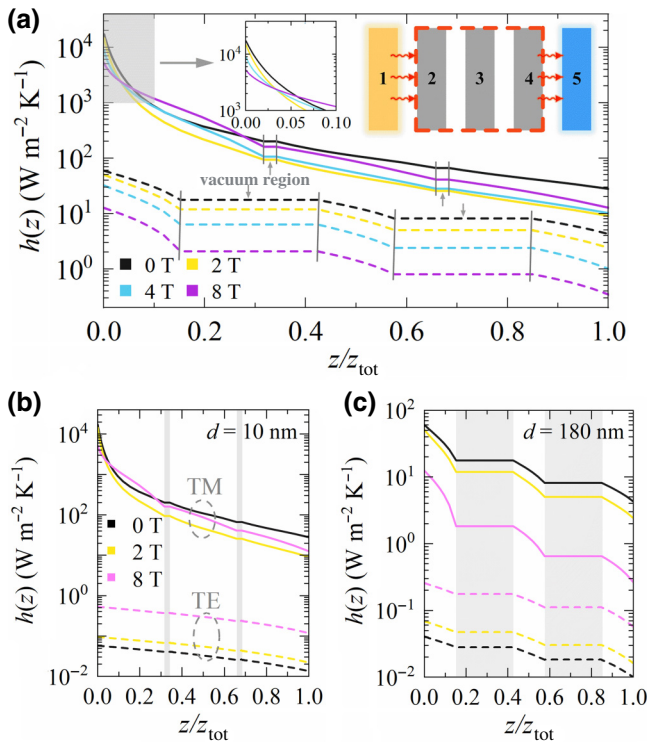
FIG. 4. (a) Magnetic field dependence of the spatial profile of the total energy flux across the modulator slabs for the gap sizes $d = 10$ nm (solid curves) and $d = 180$ nm (dashed curves). The vacuum regions where the fluxes are not dissipated are delimited by the vertical gray lines. (b) Thermal contributions coming from TM- (solid curves) and TE-polarized modes (dashed curves) with $B = 0, 2, 8$ T for $d = 10$ nm. The vacuum regions are marked by gray shaded areas. (c) Same as in (b), but for $d = 180$ nm. The cold terminal temperature is fixed at 300 K.

dependency on the field intensity, standing in stark contrast to the results for other gap sizes. More specifically, for $d = 10$ nm, its heat-transfer coefficient drops rapidly to a global minimum as the magnetic field increases to about 2.3 T, but then yields a progressive rise as the field becomes intenser; by contrast, the transfer coefficients for wider gaps ($d \geq 25$ nm) always decreases monotonically with the field and finally remains almost constant.

The above difference in the heat-transfer coefficients leads to an interesting TMR behavior: strong magnetic fields typically favor the formation of a higher thermal resistance with respect to weak ones, yet this correlation may not hold for very compact configurations. As shown in Fig. 3(b), where the ratios of the thermal resistance at finite fields to that at zero fields versus the magnetic field intensity are plotted for the same d as in Fig. 3(a), only for the very compact case ($d = 10$ nm), the TMR reaches its maximum of approximately 240% with a moderate magnetic field of 2.3 T, but subsequently drops below 100% as the field further increases up to around 8 T. Such a nonmonotonic change of the TMR has not been observed in either

a chain of interacting InSb dipoles [34] or between two identical planar MO structures [11,45–47], both of which highlight the peculiarity of energy transport in macroscopic multibody architectures. Additionally, we note that when d is appropriately increased, the application of strong fields of above 6 T actually induces a significantly larger resistance (compared to weak fields). Under such fields, the TMR magnitude can reach above 1000% for $d \geq 100$ nm, obviously surpassing those induced previously in planar MO two-body configurations [11,44–48]. From this we can roughly judge that the production of the large TMR here is linked to the interacting degree of those MO slabs.

In order to identify the origin for the observed TMR phenomena, in Fig. 4(a) we present the spatial profiles of absorbed heat fluxes inside the intermediate modulators (i.e., slab 2, 3 and 4, sketched in the upper right corner of the panel), in the presence of magnetic fields of the strengths $B = 0, 2, 4$, and 8 T, considering $d = 10$ nm (solid curves) and $d = 180$ nm (dashed curves). The position coordinate z has been nomalized by the total transport distance of fluxes (z_{tot}) and, since radiative energy is not dissipated when traveling through the vacuum regions (between slab 2 and 3, as well as slab 3 and 4), the spatial profiles within these regions become horizontal as marked in Fig. 4(a). The first thing to notice is that, for both gap sizes, the near-field fluxes generated by tunneling from the hot slab 1 into slab 2 (corresponding to $z/z_{tot} = 0$) are more pronouncedly inhibited for stronger magnetic fields, which is very akin to what was observed between two infinite InSb slabs [11]. This field-induced reduction of energy fluxes in the near field is undoubtedly due to fact that the small wave-vector HMs induced by fields progressively replace the large wave-vector surface modes at zero fields, leading to less effective transport across vacuum gaps. But the situation subsequently becomes different. It is interesting to notice that, for the case of a 10-nm gap, the flux profile produced by applying magnetic fields up to 8 T clearly intersects with the zero-field one (inside slab 2), meaning that, within the intersection region, the presence of fields instead enhances transport of near-field fluxes. Note that this singular field-induced enhancement phenomenon does not occur when the field is reduced to 2 T. Under this moderate field, the radiative energy flux undergoes the most significant decrease after traveling through all the intermediate slabs (corresponding to $z/z_{tot} = 1$), thereby maximizing the thermal resistance. By contrast, when the MO slabs are no longer sufficiently close to each other, the attenuation trend of the spatial profiles for different applied fields becomes nearly identical to that for the zero field, supported by the results for $d = 180$ nm. In this case, strong magnetic fields naturally induce the most pronounced thermal inhibition effect at any positions, associated with the fact that they have already reduced the initial fluxes to the maximum extent.
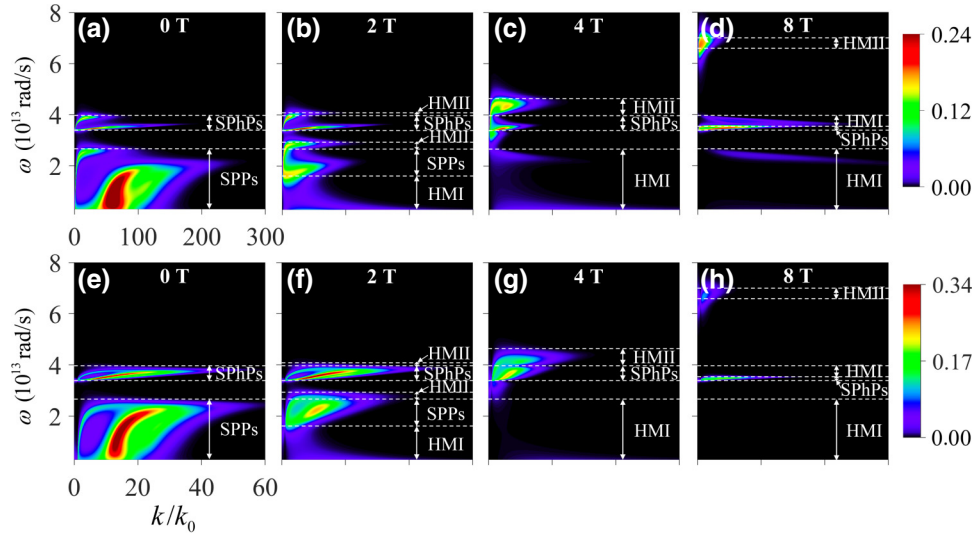
FIG. 5.   Photonic transmission probability for TM polarization from slab 1 to slab 5, $\mathcal{T}_{1\to 5}^{p}$, with respect to frequency ω and parallel wave vector k (normalized by $k_0 = \omega/c$) in the presence of the magnetic field of the strengths $B = 0, 2, 4, 8$ T. Upper (lower) panels correspond to the gap size $d = 10$ nm ($d = 180$ nm). Frequency regions corresponding to surface modes (SPPs and SPhPs) and hyperbolic modes are delimited by the horizontal white dashed lines.

In Figs. 4(b) and 4(c), we further present the thermal contributions coming from TM- (solid curves) and TE-polarized modes (dashed curves) for $d = 10$ and 180 nm, respectively, under the application of fields of 0, 2, 8 T. Incidentally, considering that polarization conversion [73] might play a role for heat transport in certain systems involving anisotropic media whose permittivity tensor has complex off-diagonal components, we have checked that the contributions from polarization conversion in our considered system is indeed insignificant. Together with Fig. 4(a), one can now clearly see that the modifications to the spatial profiles of total energy fluxes can be entirely attributed to the magnetic field effect on the TM-polarized evanescent modes (which plays a dominant role). It should also be pointed out that the presence of fields simultaneously gives rise to a moderate increase in the contribution from TE polarization, which may have consequences, as shown later in Sec. V.

To elucidate the differences between the energy-flux profiles of different gap configurations and gain more insights into the underlying physics, we next analyze the TM-polarized transmission probability from the hot terminal to the cold one, $\mathcal{T}_{1\to 5}^{p}$, shown in the upper (lower) panels of Fig. 5 for $d = 10$ nm ($d = 180$ nm), in the presence of different magnetic fields. In each panel, we have marked the frequency ranges that support SPPs, SPhPs, and HMs (HMI and HMII) when the planar InSb is subjected to the corresponding magnitude of the applied field.

Let us focus first on the discussion of the zero-field results. By comparing the photonic transmission probability without magnetic fields of Figs. 5(a) and 5(e), we discover that, different from $d = 10$ nm, the

transmission bright bands for $d = 180$ nm follow the dispersion law of cavity surface modes nicely [10]. The reason for this can be found by analyzing the radiation penetration depth, l. In the electrostatic limit, the penetration depth of an evanescent wave can be approximated by $l \approx k^{-1}$ [10,74]. For the considered many-body geometry, only thermal evanescent waves with $l \geq d$ are able to tunnel between two adjacent slabs (e.g., slab 1 and slab 2), such that the largest contributing wave vector, which dominates near-field heat transport, can be approximated as $k_{max} \approx d^{-1}$, with an associated penetration depth $l \approx d$. According to this relationship, one can judge that when $d = 10$ nm, the corresponding l is significantly smaller than the given slab thickness ($\delta = 100$ nm), in which case the dominant surface modes at the interfaces on both sides of those intermediate slabs do not couple within them, thus leading to the transmission bands in Fig. 5(a) resembling uncoupled dispersion laws of single surfaces [75,76]. This in turn explains the exponential decay of the zero-field energy flux observed for this particularly small value of d in Fig. 4. Conversely, l will be obviously larger than δ if d is altered to 180 nm, which enables the internal coupling of the evanescent fields of the surface modes from the intermediate slab, i.e., forming cavity modes within the modulators, as evidenced by Fig. 5(e). From the above analysis, we conclude that the correlation between the gap size and the slab thickness determines whether the zero-field cavity surface modes can occur within the modulating slabs.

We next turn our focus to the modifications of the transmission probability under the action of external magnetic fields. From Fig. 5 it is apparent that, as fields increase, the frequency regions supporting HMs progressively replace
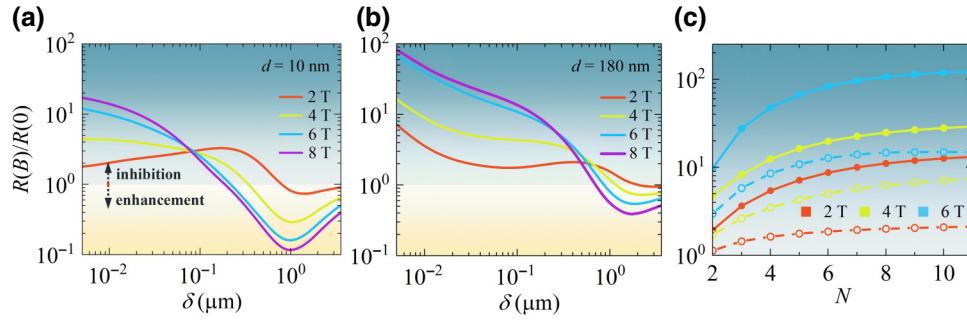
FIG. 6. (a),(b) Ratio of the thermal resistance $R(B)/R(0)$ at finite fields to the one at zero fields as a function of the slab thickness δ for various magnetic field strengths, choosing (a) $d = 10$ nm and (b) $d = 180$ nm. (c) Number dependence of $R(B)/R(0)$ for configurations comprising N InSb slabs with $\delta = 5$ nm (solid curves) and $\delta = 100$ nm (dashed curves), separated by $d = 180$ nm, with $B = 2, 4, 6$ T. The cold terminal temperature is fixed at 300 K.

the ones initially supporting surface modes, namely, the HMs will gradually dominate energy transport in the considered MO system. However, very distinct transmission behaviors are observed for two kinds of different gap sizes, as anticipated. For that very small gap ($d = 10$ nm), as fields increase to 8 T, we see two narrow transmission bands of HMs with the wave-vector cutoffs that are pronouncedly larger than the case of $B = 2$ T and even comparable to those of surface modes at zero fields [Figs. 5(a)–5(d)]. The presence of such hyperbolic bright bands means that the strong magnetic field is not as effective in inhibiting heat transport as the moderate field [see Eq. (13)], accounting for why the optimal TMR occurs with an around 2-T field when $d = 10$ nm. However, this result seems to contradict magnetic field behaviors that are usually observed between two MO planar structures [11,45–47], where strong fields always lead to the appearance of HMs with an intrinsic wave-vector cutoff much smaller than that of disappeared surface modes. To clarify this point, let us first recall the result of Fig. 4(a) for $d = 10$ nm. There, the energy flux at zero fields decays exponentially, associated with the fact that surface modes from the intermediate slabs (with δ notably larger than d) cannot couple within them to form cavity modes; however, the application of strong magnetic fields leads to fluxes decaying at a slower rate, so that they even may enhance transport of heat, albeit only within slab 2. Based on this result and together with our previous analysis of the zero-field transmission probability, we can now attribute the peculiar field-induced enhancement behavior entirely to the propagating HMs, which, as fields increase, have a larger propagation capacity and larger penetration depth relative to the zero-field surface modes thanks to their intrinsic smaller wave-vector cutoffs (since $l \approx k^{-1}$). Therefore, this eventually leads to the observation of the strong-field-induced HMs that exhibit abnormally large wave-vector cutoffs comparable to zero-field surface modes.

On the other hand, when the gap size is effectively increased, as $d = 180$ nm, we see in Figs. 5(e)–5(h) that the

transmission of the HMs becomes extremely weak as the applied field gets intense. We point out that such a gap size will significantly attenuate the tunneling of field-induced HMs (which are indeed more susceptible to the gap variation as compared to the large wave-vector surface modes), leading to quite weak fluxes in Fig. 4(a). On the other hand, we recall that this wider gap (with respect to δ) simultaneously favors the formation of zero-field cavity modes as a consequence of the coupling of the evanescent fields within the modulating slabs. The combination of these two points leads to the conclusion that the applied magnetic field now serves to transform an effective energy tunneling arising from zero-field cavity surface modes into a poor tunneling mediated by field-induced HMs. This remarkable transformation, which benefits from the introduction of the intermediate slabs, is the key for the emergence of a large TMR ($> 1000\%$) in the current MO configuration.

Upon the above analysis, we expect that the satisfaction of the geometric condition $d > \delta$ could be necessary for maximizing the TMR effect in the MO configuration under consideration. To test this idea, we now take two gap sizes $d = 10$ and 180 nm as examples, and plot their resistance ratios $R(B)/R(0)$ as a function of the slab thickness δ, varying from 5 nm to 3.5 μm, for different strengths of magnetic fields in Figs. 6(a) and 6(b), respectively. Incidentally, we do not consider the results for the thickness range of $\delta < 5$ nm, for which the nonlocal effect may become non-negligible [77]. It is immediately seen that, for both given gap sizes, $R(B)/R(0)$ reaches the maximum value when all InSb slabs have the smallest thickness ($\delta = 5$ nm) and are subjected to the strongest magnetic field ($B = 8$ T). Meanwhile, we notice that this value for $d = 180$ nm corresponds to a very huge TMR as high as approximately 10 000%, which is truly remarkable when we compare it to the resistances obtained in existing MO systems with similar magnetic fields (never exceeding the order of 1000%). [11,34,44–48]. The observed XTMR effect arises exactly from the fact that a suitably larger d (with respect to δ) is more advantageous for inhibiting the effective tunneling driven by zero-field cavity surface

modes by applying a sufficiently strong external field, as explained earlier. Therefore, it is not surprising that when the system comprises very thin InSb slabs, the XTMR can occur over a relatively wide range of d (see Supplemental Material [70]).

Another remarkable field behavior is that the application of magnetic fields can even enhance heat transport along the whole system, as is more evident from the 10-nm gap results, where, as shown in Fig. 6(a), the presence of sufficiently high fields ($B \geq 6$ T) leads to $R(B)/R(0)$ being obviously less than 1 and a negative TMR up to over -80% at sufficiently large thicknesses of near 1 μm. This result further indicates that the magnetic field may totally change its role in heat transport when d is much smaller than δ. This arises from the fact that the slabs with large thicknesses hinder the coupling of zero-field surface modes inside of them, leading to a low tunneling, which is, in turn, effectively enhanced by the field-induced HMs due to their larger penetration depth. Note that the negative thermal resistance induced here is entirely subjected to the intrinsic small wave-vector HMs, differing from what was found in the asymetric MO two-body configurations [44,48], which could inspire one to desigin fascinating MO architectures to assist energy transport.

So far, we have demonstrated the possiblity of inducing a XTMR in MO InSb few-slab configurations with relatively strong magnetic fields. Let us finish this section by displaying that appropriately adjusting the number of MO slabs is an feasible technique to reduce the required field, which could be more appealing for practial applications [30]. In Fig. 6(c) we present the number dependence of $R(B)/R(0)$ for configurations comprising N slabs with the thicknesses $\delta = 5$ nm (solid curves) and 100 nm (dashed curves), separated by $d = 180$ nm. This plot shows that even if the applied field and certain structual parameters (d and δ) are fixed, one can still effectively elevate the resistance by optimizing the slab number. This therefore allows for the production of a higher TMR upon the application of a lower magnetic field. For instance, when our architecture consists of $N = 8$ InSb slabs with a 5 nm thickness, the TMR magnitude now reaches up to about 10 000% with a 6-T field and about 1000% even with a moderate 2-T field.

V. MAGNETIC-FIELD-DRIVEN TRANSITION OF TRANSPORT REGIMES IN MO MANY-SLAB CONFIGURATIONS

Unlike radiative many-dipole systems that only allow for the occurrence of a superdiffussive regime of heat transport [49,51,52], practial systems consisting of numerous macroscopic planar objects may exhibit more complex transport behaviors. As recently demonstrated in Ref. [53], in a linear many-slab system purely made of polar dielectric SiC (supporting strong SPhPs), its transport regime

undergoes a transition between superdiffussive and ballistic, when the system density is substantially enhanced. Motivated by this finding, in this section we shall pay our attention to examining how heat carried by thermal photons is transported in many-body configuration comprising MO planar slabs, with particular attention to the possibility to induce a ballistic transport by applying an external magnetic field. For our purposes, let us now consider our system featuring a considerably large number of InSb slabs, which are necessary and useful for identifying transport regimes, as illustrated below.

For one-dimensional planar radiative systems with a small temperature difference, by reasonably assuming that the heat-transfer coefficient $h_{ij} \sim 1/z_{ij}^{\gamma}$ (where z_{ij} is the separation between slab i and slab j) it has been demonstrated that, in the thermodynamic limit $N \to \infty$ and the total length of the system $L \to \infty$, the positions of slabs can be continuously described by $z_j \to z$, so that $T_j \to T(z)$ and the total flux received by slab j is given by $\varphi_j = \sum_{i \neq j} \varphi_{ij} \to \varphi(z) \sim (-\Delta)^{\gamma - 1/2} T(z)$ (see detailed derivations in Ref. [53]). The term $(-\Delta)^{\gamma - 1/2}$ is the fractional Laplacian, which, by introducing $\gamma = \alpha + 1$, can be defined as [29,78]

$$(-\Delta)^{\alpha/2} T(z) = c_\alpha \mathrm{PV} \int_{-\infty}^{\infty} \frac{T(z) - T(z')}{|z - z'|^{1+\alpha}} dz', \quad (15)$$

with the constant

$$c_\alpha = \frac{2^{-\alpha} \pi^{3/2}}{\Gamma(1 + \alpha/2) \Gamma[(1 + \alpha)/2] \sin(\alpha \pi /2)},$$

$\Gamma(x)$ being the Gamma function, and PV stands for the principal value. Equation (15) establishes a relationship between the asymptotic, large-distance behavior of transfer coefficients and the heat-transport regime. Specifically, when $\gamma = 3$, the fractional Laplacian degenerates into its classical form, so the transport regime is diffusive, whereas for $\gamma = 1$, the fractional Laplacian approaches the identity operator, so that transport becomes ballistic. Finally, when $1 < \gamma < 3$ the transport is superdiffusive.

We are going to consider our many-body geometry consisting of $N = 65$ n-doped InSb planar slabs with an identical thickness of $\delta = 200$ nm. The reasons for this thickness setup are twofold. Firstly, we have checked that, under this thickness, radiative energy will undergo a sufficiently strong decay along the entire system, allowing us to identify the type of heat-transport regimes exactly. Secondly, this thickness setup aligns with that of Ref. [53], which is also convenient for the comparison and discussion of the difference in transport regimes between the semiconductor system under study and the dielectric system of interest in Ref. [53].

Figure 7(a) shows the heat-transfer coefficient h_{ij} between the central slab ($i = 33$) and another one ($j > 33$)
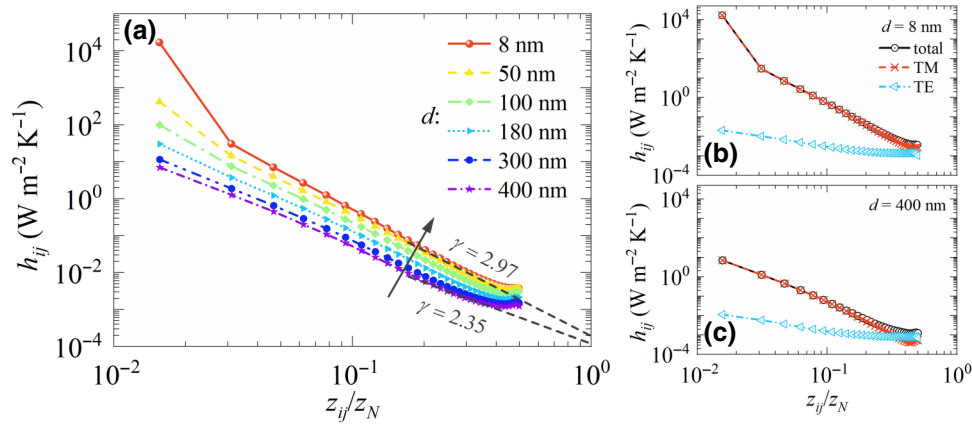
FIG. 7. (a) Heat-transfer coefficients h_{ij} with respect to the normalized separation z_{ij}/z_N, for different gap sizes d in the absence of magnetic fields. Dashed lines show the asymptotic behavior of $h_{ij} \sim 1/z_{ij}^\gamma$ at large separation distances. The value of γ stands for the nature of the heat-transport regime. (b) Thermal contributions from TM- and TE-polarized modes for $d = 8$ nm. (c) Same as in (b), but for $d = 400$ nm. The temperature difference between the two terminals $\Delta T = T_1 - T_{65} = 10$ K, with $T_{65} = 300$ K.

as a function of their separation distance Δz (normalized by z_N) in the absence of magnetic fields. From this plot the influence of the system density on the asymptotic, large-distance behavior of h_{ij} is intuitive: as we gradually reduce d from 400 to 8 nm to render the system rather dense, h_{ij} scales as $1/z_{ij}^\gamma$, with an exponent γ that monotonically increases from 2.35 to 2.97, indicating that significantly densifying our considered system will lead to its radiative transport changing from a unambiguously superdiffusive regime to a regime approaching diffusion. Note that the anomalous variations in h_{ij} at the end of the curves are a result of finite-size effects [52,53], and are not taken into account in the scaling analysis. The phenomenon observed here stands in sharp contrast to what has been found in the SiC many-slab configuration in which a nonmonotonic transition, from superdiffusive to ballistic, arises as the system gradually becomes rather dense [53]. It follows that the occurrence of ballistic transport in macroscopic planar many-body systems depend strongly on not only structural parameters, but also on material components.

To shed light on this difference, let us briefly review the origin of the transition in the SiC system. It is associated with a fundamental change in the polarization of the dominant modes, from TM to TE polarization in the dense case [53]. We argue that this unique variation is entirely determined by the intrinsic characteristics of this kind of polar dielectric, which should be an uncommon phenomenon, as it does not occur for magnetic semiconductors as InSb (even though it also supports strong surface states in the absence of magnetic fields). As evidenced in Figs. 7(b) and 7(c), where we extract the thermal contributions from TM- and TE-polarized modes for $d = 8$ and 400 nm, respectively, it is clearly seen that, for the InSb many-slab configuration, TM modes are exclusively dominant when d is reduced significantly. On the other hand,

we need to emphasize that, when a radiative many-slab system becomes denser, the penetration depth of the supported surface modes is decreasing (as explained in the previous section and discussed in Ref. [79]). Consequently, when our system is gradually densified, the zero-field surface modes of InSb slabs tend to couple only between neighboring slabs, accounting for a diffusionlike regime in Fig. 7(a).

In addition, the results of Figs. 7(b) and 7(c) simultaneously suggest that, for the system under consideration, the large-distance heat fluxes originating from TM modes decay more rapidly compared to those from TE modes, hardly subjected to gap sizes, which leads to the exponent γ in the scaling of the total h_{ij} being obviously greater than 1. From this we deduce that involving as many TE modes as possible in carrying heat could be necessary for inducing a transition from superdiffusive to ballistic regime.

Can an applied magnetic field induce a ballistic transport? To answer it, we present the heat-transfer coefficients with respect to the normalized separation distance for three different gap sizes in the presence of magnetic fields, shown in Figs. 8(a)–8(c), where the zero-field results are added as a reference (black curves). We observe that, in all the cases ($d = 8$, 100, 400 nm), the exponent γ in the scaling of h_{ij} under the action of strong fields is clearly smaller as compared to the zero-field results. Of note, for the case of $d = 400$ nm, γ has decreased to 1 under the application of an 8-T magnetic field [Fig. 8(c)], indicating that heat transport becomes unambiguously ballistic. By further tracing the thermal contributions of TM- and TE-polarized modes with $B = 8$ T, shown in those insets of Fig. 8, we confirm that this field-induced transition of transport regimes (from superdiffusive to ballistic) stems from TE modes acting as a primary heat-transport channel
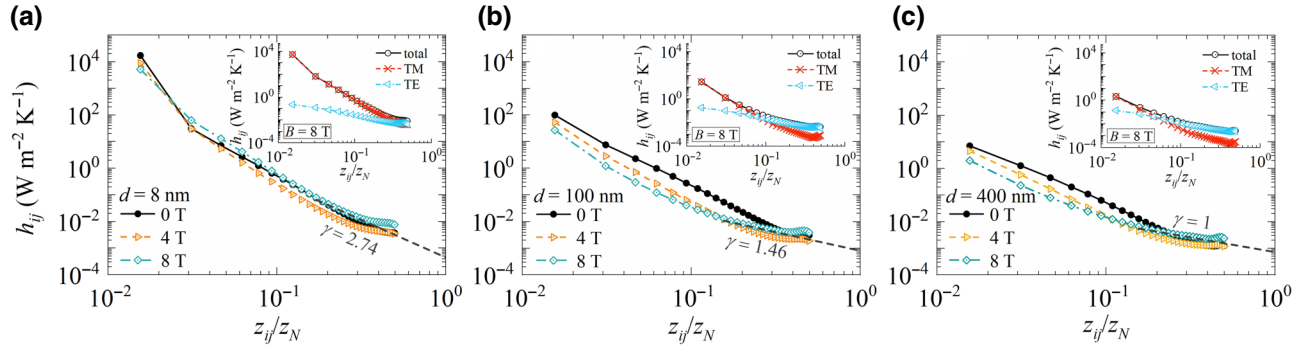
FIG. 8. Heat-transfer coefficients h_{ij} with respect to the normalized separation z_{ij}/z_N, for three different values of the gap sizes of (a) 8 nm, (b) 100 nm, and (c) 400 nm, in the presence of magnetic fields of the strengths $B = 0, 4, 8$ T. The insets show h_{ij} versus z_{ij}/z_N with $B = 8$ T, as well as thermal contributions coming from TM- and TE-polarized modes for the corresponding gap size. The temperature difference between the two terminals $\Delta T = T_1 - T_{65} = 10$ K, with $T_{65} = 300$ K.

at large transport distances. Note that this heat-transport mechanism in the complex system featuring numerous InSb slabs subjected to magnetic fields should be distinguished from its two- or few-body counterparts where, as discussed in the previous section, TM modes typically dominate. Note also that although the transition driven by magnetic fields here is also associated with the variation in the polarization of dominant modes, as previously found in the SiC system, the mechanisms behind both are radically different. We argue that the reason that TE-polarized modes dominate large-distance heat transport in the current InSb system are twofold. First and foremost, when these MO slabs are not dense and subjected to strong magnetic fields, the field-induced HMs featuring intrinsic small wave vectors, highly replacing the zero-field surface modes with large wave vectors, decay dramatically over a large distance, such that TM modes now fail to dominate large-distance heat transport unlike the zero-field case [see Fig. 7(c) and the inset of Fig. 8(c)]. Moreover, the application of magnetic fields also has an appreciable enhancement effect on radiative energy originating from TE modes (note that this field behavior now becomes non-negligible), as clearly demonstrated by the transmission probability results within the Supplemental Material [70]. Overall, the mechanism of ballistic transport magnetically induced here is relatively intricate, which displays the rich physics in macroscopic many-body systems again.

VI. REMARKS

Let us now discuss some potential applications of our predicted thermomagnetic effects. In a well-crafted MO planar many-body architecture, the application of an external magnetic field allows one to generate an extremely large resistance, so that energy transport governed by photons could be completely hold in an "OFF" state. This contrasts with the zero-field case, for which transport could

be efficient (as we have demonstrated), corresponding to an "ON" state. Therefore, this implies that the XTMR effect could be exploited to design a thermal magnetic switch [80] that operates with exceptional efficiency. Moreover, the XTMR should be more competitive and trustworthy than the GTMR [34] for the locally measuring heat fluxes or temperatures, which is, in turn, of significance for developing thermal magnetic sensors. In addition, as shown in Ref. [53], the photonic relaxation process in out-of-thermal-equilibrium systems at the timescale could, in principle, shorten siginifcantly when transitioning from superdiffusive to ballistic transport. Based on this, we anticipate that this transition induced by external magnetic fields in periodic MO slab configurations would offer alternative perspectives to design energy devices capable of fast or even ultrafast thermal transport.

VII. CONCLUSIONS

In conclusion, we have predicted two novel thermomagnetic effects related to near-field RHT in macroscopic planar MO many-body systems. First, we have predicted a XTMR, which is a thermal analogue of the XMR that is gaining great attention in spintronics, in a simple MO configuration comprising only a few interacting InSb planar slabs. It was found that when these MO slabs are very thin and simultaneously separated by relatively large vacuum gaps, the XTMR as high as the order of 10 000% can be induced at room temperature by applying an external magnetic field up to 8 T. The underlying mechanism is that under such dilute multibody architectures, the application of a sufficiently strong magnetic field leads to a very low-energy tunneling arising from field-induced hyperbolic modes, replacing the effective tunneling driven by zero-field cavity surface modes. We also showed that it is feasible to lower the necessary field appropriately by adding a certain number of MO slabs. Furthermore, a negative GTMR (of

around –80%) was observed when the InSb slabs are sufficiently thick but separated by small gaps (note that this geometric condition is the exact opposite of that for which the XTMR occurs). We elucidated that this intriguing phenomenon also depends strongly on the magnetic-field-induced HMs, whose large penetration depth renders them possible to effectively improve the low zero-field tunneling behavior arising from the uncoupled surface modes within the thick intermediate slabs.

We further examined the heat-transport regime in a linear MO many-slab configuration, with a particular focus on the modification of transport regimes with external magnetic fields. In stark contrast to the SiC many-slab result, increasing the density of an InSb many-slab configuration at zero fields leads to an alteration of radiative transport from a superdiffusive regime to a diffusionlike one, indicating that the transport process in planar multibody systems depends on both the structural parameters and material components. Of note, we have predicted a magnetic-field-driven transition from superdiffusive to ballistic transport. This peculiar thermomagnetic phenomenon was shown to be associated with a complete change in the dominant modes, switching from TM- to TE-polarized modes. Such a change is because the magnetic field, on one hand, induces the small wave-vector HMs, which decay significantly over large distances for a relatively dilute system, fundamentally responsible for a loss of thermal dominance of TM modes, while on the other hand, enhancing the large-distance probability of TE modes.

In all our calculations, we have assumed perfectly flat surfaces. But in practice surface roughness is an unavoidable issue. Prior studies [81,82] have theoretically and experimentally shown that roughness plays an insignificant role in heat transport between two slabs separated by subwavelength vacuum gaps when its amplitude is notably smaller than the gap size. Therefore, our results are expected to be valid as long as surface roughness has an amplitude clearly smaller than vacuum gaps, which is achievable by using current technology.

So, in short, our predicted near-field thermomagnetic effects would have significant implications for the nanoscale thermal management of multibody architectures. Moreover, our work once again shows the potential for numerous rich physical phenomena to occur in macroscopic many-body systems with specific geometries and materials, which would inspire the exploration of captivating transport behaviors linked to thermal photons in complex architectures in the near future.

ACKNOWLEDGMENTS

[1] A. Narayanaswamy and G. Chen, Surface modes for near field thermophotovoltaics, Appl. Phys. Lett. **82**, 3544 (2003).

[2] A. Fiorino, L. Zhu, D. Thompson, R. Mittapally, P. Reddy, and E. Meyhofer, Nanogap near-field thermophotovoltaics, Nat. Nanotechnol. **13**, 806 (2018).

[3] R. Mittapally, A. Majumder, P. Reddy, and E. Meyhofer, Near-field thermophotovoltaic energy conversion: Progress and opportunities, Phys. Rev. Appl. **19**, 037002 (2023).

[4] L. Zhu, A. Fiorino, D. Thompson, R. Mittapally, E. Meyhofer, and P. Reddy, Near-field photonic cooling through control of the chemical potential of photons, Nature (London) **566**, 239 (2019).

[5] S. Buddhiraju, W. Li, and S. Fan, Photonic refrigeration from time-modulated thermal emission, Phys. Rev. Lett. **124**, 077402 (2020).

[6] D. D. Feng, S. K. Yee, and Z. M. M. Zhang, Near-field photonic thermal diode based on hBN and InSb films, Appl. Phys. Lett. **119**, 181111 (2021).

[7] Q. Z. Li, Q. Chen, and B. Song, Giant radiative thermal rectification using an intrinsic semiconductor film, Mater. Today Phys. **23**, 100632 (2022).

[8] A. I. Volokitin and B. N. J. Persson, Near-field radiative heat transfer and noncontact friction, Rev. Mod. Phys. **79**, 1291 (2007).

[9] S.-A. Biehs, M. Tschikin, and P. Ben-Abdallah, Hyperbolic metamaterials as an analog of a blackbody in the near field, Phys. Rev. Lett. **109**, 104301 (2012).

[10] B. Song, Y. Ganjeh, S. Sadat, D. Thompson, A. Fiorino, V. Fernández-Hurtado, J. Feist, F. J. Garcia-Vidal, J. C. Cuevas, P. Reddy, and E. Meyhofer, Enhancement of near-field radiative heat transfer using polar dielectric thin films, Nat. Nanotechnol. **10**, 253 (2015).

[11] E. Moncada-Villa, V. Fernández-Hurtado, F. J. García-Vidal, A. García-Martín, and J. C. Cuevas, Magnetic field control of near field radiative heat transfer and the realization of highly tunable hyperbolic thermal emitters, Phys. Rev. B **92**, 125418 (2015).

[12] V. Fernández-Hurtado, F. J. García-Vidal, S. Fan, and J. C. Cuevas, Enhancing near-field radiative heat transfer with Si-based metasurfaces, Phys. Rev. Lett. **118**, 203901 (2017).

[13] M. Ghashami, H. Geng, T. Kim, N. Iacopino, S. K. Cho, and K. Park, Precision measurement of phonon-polaritonic near-field energy transfer between macroscale planar structures under large thermal gradients, Phys. Rev. Lett. **120**, 175901 (2018).

[14] J. Yang, W. Du, Y. Su, Y. Fu, S. Gong, S. He, and Y. Ma, Observing of the super-Planckian near-field thermal radiation between graphene sheets, Nat. Commun. **9**, 1 (2018).

[15] P. S. Venkataram, S. Molesky, W. Jin, and A. W. Rodriguez, Fundamental limits to radiative heat transfer: The limited role of nanostructuring in the near-field, Phys. Rev. Lett. **124**, 013904 (2020).

[16] L. Rincón-García, D. Thompson, R. Mittapally, N. Agraït, E. Meyhofer, and P. Reddy, Enhancement and saturation of near-field radiative heat transfer in nanogaps between metallic surfaces, Phys. Rev. Lett. **129**, 145901 (2022).

[17] Y. Du, J. Peng, Z. Shi, and J. Ren, Twist-induced near-field radiative heat switch in hyperbolic antiferromagnets, Phys. Rev. Appl. **19**, 024044 (2023).

[18] P. Ben-Abdallah, S.-A. Biehs, and K. Joulain, Many-body radiative heat transfer theory, Phys. Rev. Lett. **107**, 114301 (2011).

[19] L. Zhu and S. Fan, Persistent directional current at equilibrium in nonreciprocal many-body near field electromagnetic heat transfer, Phys. Rev. Lett. **117**, 134303 (2016).

[20] E. Tervo, M. Francoeur, B. Cola, and Z. M. Zhang, Thermal radiation in systems of many dipoles, Phys. Rev. B **100**, 205422 (2019).

[21] K. Asheichyk and M. Krüger, Radiative heat transfer with a cylindrical waveguide decays logarithmically slow, Phys. Rev. Lett. **129**, 1170605 (2022).

[22] R. Messina, M. Antezza, and P. Ben-Abdallah, Three-body amplification of photon heat tunneling, Phys. Rev. Lett. **109**, 244302 (2012).

[23] Y. H. Kan, C. Y. Zhao, and Z. M. Zhang, Enhancement and manipulation of near-field radiative heat transfer using an intermediate modulator, Phys. Rev. Appl. **13**, 014069 (2020).

[24] I. Latella, P. Ben-Abdallah, and M. Nikbakht, Radiative thermal rectification in many-body systems, Phys. Rev. B **104**, 045410 (2021).

[25] P. Ben-Abdallah and S.-A. Biehs, Near-field thermal transistor, Phys. Rev. Lett. **112**, 044301 (2014).

[26] J. Song, L. Lu, B. Li, B. Zhang, R. Hu, X. Zhou, and Q. Cheng, Thermal routing via near-field radiative heat transfer, Int. J. Heat Mass Transfer **150**, 119346 (2020).

[27] C. Guo, B. Zhao, D. Huang, and S. Fan, Radiative thermal router based on tunable magnetic Weyl semimetals, ACS Photonics **7**, 11 (2020).

[28] J. C. Cuevas and F. J. Garca-Vidal, Radiative heat transfer, ACS Photonics **5**, 3896 (2018).

[29] S.-A. Biehs, R. Messina, P. S. Venkataram, A. W. Rodriguez, J. C. Cuevas, and P. Ben-Abdallah, Near-field radiative heat transfer in many-body systems, Rev. Mod. Phys. **93**, 025009 (2021).

[30] Z. Zhang and L. Zhu, Nonreciprocal thermal photonics for energy conversion and radiative heat transfer, Phys. Rev. Appl. **18**, 027001 (2022).

[31] A. Ott, R. Messina, P. Ben-Abdallah, and S.-A. Biehs, Magneto thermoplasmonics: From theory to applications, J. Photonics Energy **9**, 032711 (2019).

[32] P. Ben-Abdallah, Photon thermal Hall effect, Phys. Rev. Lett. **116**, 084301 (2016).

[33] C. Guo, Y. Guo, and S. Fan, Relation between photon thermal Hall effect and persistent heat current in nonreciprocal radiative heat transfer, Phys. Rev. B **100**, 205416 (2019).

[34] I. Latella and P. Ben-Abdallah, Giant thermal magnetoresistance in plasmonic structures, Phys. Rev. Lett. **118**, 173902 (2017).

[35] J. M. Ziman, *Principles of the Theory of Solids* (Cambridge University Press, New York, 1972).

[36] A. B. Pippard, *Magnetoresistance in Metals* (Cambridge University Press, Cambridge, UK, 1989).

[37] M. N. Ali, J. Xiong, S. Flynn, J. Tao, Q. D. Gibson, L. M. Schoop, T. Liang, N. Haldolaarachchige, M. Hirschberger, N. P. Ong, and R. J. Cava, Large, non-saturating magnetoresistance in WTe_2, Nature (London) **514**, 205 (2014).

[38] Y. Y. Wang, H. Zhang, X.-Q. Lu, L.-L. Sun, S. Xu, Z.-Y. Lu, K. Liu, S. Zhou, and T.-L. Xia, Extremely large magnetoresistance and electronic structure of TmSb, Phys. Rev. B **97**, 085137 (2018).

[39] S. Zhang, Q. Wu, Y. Liu, and O. Yazyev, Magnetoresistance from Fermi surface topology, Phys. Rev. B **99**, 035142 (2019).

[40] J. Bannies, E. Razzoli, M. Michiardi, H.-H. Kung, I. S. Elfimov, M. Yao, A. Fedorov, J. Fink, C. Jozwiak, A. Bostwick, E. Rotenberg, A. Damascelli, and C. Felser, Extremely large magnetoresistance from electron-hole compensation in the nodal-loop semimetal ZrP_2, Phys. Rev. B **103**, 155144 (2021).

[41] A. Singh, S. Sasmal, K. K. Iyer, A. Thamizhavel, and K. Maiti, Evolution of extremely large magnetoresistance in a Weyl semimetal, WTe_2 with Ni-doping, Phys. Rev. Mater. **6**, 124202 (2022).

[42] Y.-Y. Lv, X. Li, L. Cao, D. Lin, S.-H. Yao, S.-S. Chen, S.-T. Dong, J. Zhou, Y. B. Chen, and Y.-F. Chen, Tunable resistance or magnetoresistance cusp and extremely large magnetoresistance in defect-engineered $HfTe_{5-\delta}$ single crystals, Phys. Rev. Appl. **9**, 054049 (2018).

[43] J. Zhang, J. M. Ok, Y.-Y. Pai, J. Lapano, E. Skoropata, A. R. Mazza, H. Li, A. Huon, S. Yoon, B. Lawrie, M. Brahlek, T. Z. Ward, G. Eres, H. Miao, and H. N Lee, Extremely large magnetoresistance in high-mobility $SrNbO_3/SrTiO_3$ heterostructures, Phys. Rev. B **104**, L161404 (2021).

[44] E. Moncada-Villa and J. C. Cuevas, Magnetic field effects in the near-field radiative heat transfer between planar structures, Phys. Rev. B **101**, 085411 (2020).

[45] J. Song, Q. Cheng, L. Lu, B. Li, K. Zhou, B. Zhang, Z. Luo, and X. Zhou, Magnetically tunable near-field radiative heat transfer in hyperbolic metamaterials, Phys. Rev. Appl. **13**, 024054 (2020).

[46] E. Moncada-Villa and J. C. Cuevas, Near-field radiative heat transfer between one-dimensional magnetophotonic crystals, Phys. Rev. B **103**, 075432 (2021).

[47] B. Zhao, L. Lu, J. Song, Z. Luo, and Q. Cheng, Active control of near-field radiative heat transfer between InSb and graphene multilayered magneto-optical metamaterials, Int. J. Heat Mass Transfer **192**, 15 (2022).

[48] G. Tang, Lei Zhang, Yong Zhang, Jun Chen, and C. T. Chan, Near-field energy transfer between graphene and magneto-optic media, Phys. Rev. Lett. **127**, 247401 (2021).

[49] Philippe Ben-Abdallah, Riccardo Messina, Svend-Age Biehs, Maria Tschikin, Karl Joulain, and Carsten Henkel, Heat superdiffusion in plasmonic nanostructure networks, Phys. Rev. Lett. **111**, 174301 (2013).

[50] C. Kathmann, R. Messina, P. Ben-Abdallah, and S.-A. Biehs, Limitations of kinetic theory to describe near-field heat exchanges in many-body systems, Phys. Rev. B **98**, 115434 (2018).

[51] M. Luo, J. Zhao, and L. Liu, Near-field radiative heat transfer in a chain of nanoparticles withanother chain

in proximity, J. Quant. Spectrosc. Radiat. Transfer **243,** 106801 (2020).

[52] L. Qu, Y. Zhang, J.-L. Fang, and H.-L. Yi, Steady-state temperature distribution under near-field radiative heat transfer inside a linear chain of polaritonic nanoparticles, J. Quant. Spectrosc. Radiat. Transfer **258,** 107404 (2021).

[53] I. Latella, S.-A. Biehs, R. Messina, A. W. Rodriguez, and P. Ben-Abdallah, Ballistic near-field heat transport in dense many-body systems, Phys. Rev. B **97,** 035423 (2018).

[54] E. D. Palik, *Handbook of Optical Constants of Solids* (Academic Press, London, 1985).

[55] J.-P. Mulet, K. Joulain, R. Carminati, and J.-J. Greffet, Enhanced radiative heat transfer at nanometric distances, Microscale Thermophys. Eng. **6,** 209 (2002).

[56] L. Tang, L. M. Correa, M. Francoeur, C. Dames, Large enhancement of near-field radiative heat transfer in the dual nanoscale regime enabled by electromagnetic corner and edge modes, arXiv:2310.20356.

[57] X. Luo, H. Salihoglu, Z. Wang, Z. Li, H. Kim, X. Liu, J. Li, B. Yu, S. Du, and S. Shen, Observation of near-field thermal radiation between coplanar nanodevices with subwavelength dimensions, Nano. Lett. **24,** 5 (2024).

[58] E. D. Palik, R. Kaplan, R. W. Gammon, H. Kaplan, R. F. Wallis, and J. J. Quinn, Coupled surface magnetoplasmon-optic-phonon polariton modes on InSb, Phys. Rev. B **13,** 2497 (1976).

[59] R. Messina, P. Ben-Abdallah, B. Guizal, M. Antezza, and S.-A. Biehs, Hyperbolic waveguide for long-distance transport of near-field heat flux, Phys. Rev. B **94,** 104301 (2016).

[60] Y. H. Kan, C. Y. Zhao, and Z. M. Zhang, Near-field radiative heat transfer in three-body systems with periodic structures, Phys. Rev. B **99,** 035443 (2019).

[61] Ming-Jian He, Hong Qi, Yi-Fei Wang, Ya-Tao Ren, Wei-Hua Cai, and Li-Ming Ruan, Near-field radiative heat transfer in multilayered graphene system considering equilibrium temperature distribution, Opt. Express **27,** 16 (2019).

[62] G. T. Papadakis, C. J. Ciccarino, L. Fan, M. Orenstein, P. Narang, and S. Fan, Deep-subwavelength thermal switch via resonant coupling in monolayer hexagonal boron nitride, Phys. Rev. Appl. **15,** 054002 (2021).

[63] N. Zolghadr and M. Nikbakht, Radiative resistance at the nanoscale: Thermal barrier, Phys. Rev. B **102,** 035433 (2020).

[64] R. Messina and M. Antezza, Three-body radiative heat transfer and Casimir-Lifshitz force out of thermal equilibrium for arbitrary bodies, Phys. Rev. A **89,** 052104 (2014).

[65] I. Latella, P. Ben-Abdallah, S.-A. Biehs, M. Antezza, and R. Messina, Radiative heat transfer and nonequilibrium Casimir Lifshitz force in many-body systems with planar geometry, Phys. Rev. B **95,** 205404 (2017).

[66] L. Qu, E. Moncada-Villa, J.-L. Fang, Y. Zhang, and H.-L. Yi, Tunable magnetic field effects on the near-field radiative heat transfer in three-body systems, Phys. Rev. B **107,** 205405 (2023).

[67] K. Chen, B. Zhao, and S. Fan, Mesh: A free electromagnetic solver for far-field and near-field radiative heat transfer for layered periodic structures, Comput. Phys. Commun. **231,** 163 (2018).

[68] S. M. Rytov, Y. A. Kravtsov, and V. I. Tatarskii, *Principles of Statistical Radiophysics* (Springer-Verlag, Berlin, Heidelberg, 1989), Vol. 3.

[69] B. Caballero, A. García-Martín, and J. C. Cuevas, Generalized scattering-matrix approach for magneto-optics in periodically patterned multilayer systems, Phys. Rev. B **85,** 245103 (2012).

[70] See Supplemental Material http://link.aps.org/supplemental/10.1103/PhysRevApplied.21.064022, which includes Refs. [11,69], for the numerical calculation of the electric and magnetic Green's functions, the XTMR effect of a few-body configuration with thin InSb slabs, and the variation of transmission probability for TE and TM polarization between two InSb slabs at large separations under the action of magnetic fields.

[71] K. Joulain, J.-P. Mulet, F. Marquier, R. Carminati, and J.-J. Greffet, Surface electromagnetic waves thermally excited: Radiative heat transfer, coherence properties and Casimir forces revisited in the near field, Surf. Sci. Rep. **57,** 3 (2005).

[72] C. Guo and S. Fan, Theoretical constraints on reciprocal and non-reciprocal many-body radiative heat transfer, Phys. Rev. B **102,** 085401 (2020).

[73] C.-L. Zhou, G. Tang, Y. Zhang, M. Antezza, and H.-L. Yi, Radiative heat transfer in a low-symmetry Bravais crystal, Phys. Rev. B **106,** 155404 (2022).

[74] M. Francoeur, M. P. Mengüç, and R. Vaillon, Spectral tuning of near-field radiative heat flux between two thin silicon carbide films, J. Phys. D: Appl. Phys. **43,** 075501(2010).

[75] M. Francoeur, M. P. Mengüç, and R. Vaillon, Coexistence of multiple regimes for near-field thermal radiation between two layers supporting surface phonon polaritons in the infrared, Phys. Rev. B **84,** 075436 (2011).

[76] S.-A. Biehs and P. Ben-Abdallah, Near-field heat transfer between multilayer hyperbolic metamaterials, Z. Naturforsch. **72,** 2 (2017).

[77] H. Salihoglu, J. Shi, Z. Li, Z. Wang, X. Luo, I. V. Bondarev, S.-A. Biehs, and S. Shen, Nonlocal near-field radiative heat transfer by transdimensional plasmonics, Phys. Rev. Lett. **131,** 086901 (2023).

[78] M. F. Shlesinger, G. M. Zaslavsky, and U. Frisch, *Lévy Flights and Related Topics in Physics* (Springer-Verlag, Berlin, 1995).

[79] S. Lang, M. Tschikin, S.-A. Biehs, A. Y. Petrov, and M. Eich, Large penetration depth of near-field heat flux in hyperbolic media, Appl. Phys. Lett. **104,** 121903 (2014).

[80] S. Pajovic and S. V. Boriskina, Magnetocaloric-effect-enhanced near-field magneto-optical thermal switch, Phys. Rev. Appl. **20,** 014053 (2023).

[81] S.-A. Biehs and and J.-J. Greffet, Influence of roughness on near-field heat transfer between two plates, Phys. Rev. B. **82,** 245410 (2010).

[82] K. Kim, B. Song, V. Fernández-Hurtado, W. Lee, W. Jeong, L. Cui, D. Thompson, J. Feist, M. T. H. Reid, F. J. García-Vidal J, C. Cuevas, E. Meyhofer, and P. Reddy, Radiative heat transfer in the extreme near field, Nature (London) **528,** 387 (2015).